Corotational Instability of Inertial-Acoustic Modes in Black-Hole Accretion Discs: Non-Barotropic Flows

David Tsang[1,2]* and Dong Lai[1]*

[1] *Department of Astronomy, Cornell University, Ithaca, NY 14853, USA*
[2] *Department of Physics, Cornell University, Ithaca, NY 14853, USA*

11 May 2010

ABSTRACT

We study the effect of corotation resonance on the inertial-acoustic oscillations (p-modes) of black-hole accretion discs. Previous works have shown that for barotropic flows (where the pressure depends only on the density), wave absorption at the corotation resonance can lead to mode growth when the disc vortensity, $\zeta = \kappa^2/(2\Omega\Sigma)$ (where Ω, κ, Σ are the rotation rate, radial epicyclic frequency and surface density of the disc, respectively), has a positive gradient at the corotation radius. Here we generalize the analysis of the corotation resonance effect to non-barotropic fluids. We show that the mode instability criterion is modified by the finite radial Brunt-Väsälä frequency of the disc. We derive an analytic expression for the reflectivity when a density wave impinges upon the corotation barrier, and calculate the frequencies and growth rates of global p-modes for disc models with various α-viscosity parameterizations. We find that for disc fluids with constant adiabatic index Γ, super-reflection and mode growth depend on the gradient of the effective vortensity, $\zeta_{\rm eff} = \zeta/S^{2/\Gamma}$ (where $S \equiv P/\Sigma^\Gamma$ measures the entropy): when $d\zeta_{\rm eff}/dr > 0$ at the corotation radius, wave absorption leads to amplification of the p-mode. Our calculations show that the lowest-order p-modes with azimuthal wave number $m = 2, \; 3, \; 4, \ldots$ have the largest growth rates, with the frequencies approximately in (but distinct from) the $2:3:4\ldots$ commensurate ratios. We discuss the implications of our results for the high-frequency quasi-periodic oscillations observed in accreting black-hole systems.

Key words: accretion, accretion discs – hydrodynamics – waves – – black hole physics – X-rays: binaries

1 INTRODUCTION

High frequency quasi-periodic oscillations (QPOs) in X-ray binary systems have been observed for a number of years and may provide an important tool for studying the strong gravitational fields of black holes (see Remillard & McClintock 2006). However, the physical mechanisms that generate such X-ray variability remain unclear. One of the most appealing models for the source of QPOs is the relativistic diskoseismic oscillation model, where general relativistic effects produce trapped oscillation modes at the inner region of an accretion disc (e.g., Kato & Fukue 1980; Okazaki et al. 1987; Nowak & Wagoner 1991; see Wagoner 1999 and Kato 2001 for reviews). Other related works on black-hole diskoseismology, such as possible mode excitation and damping (e.g., Ortega-Rodriguez & Wagoner 2000; Li, Goodman & Narayan 2003; Kato 2003,2008; Tagger & Varniere 2006; Ferreira & Ogilvie 2009; Tsang & Lai 2009a), the effects of disc magnetic fields (e.g., Tagger & Pellat 1999; Fu & Lai 2009) and numerical simulations (e.g., Arras et al. 2006; Reynolds & Miller 2008; O'Neill, Reynolds & Miller 2009), as well as other ideas for high-frequecy QPOs, such as non-linear resonances (e.g. Abramowicz & Kluzniak 1999; Horak & Karas 2006; Rebusco 2008) and boundary layer oscillations (e.g. Li & Narayan 2004; Tsang & Lai 2009b), are reviewed in section 1 of Lai & Tsang (2009).

---

* Email: dtsang@astro.cornell.edu; dong@astro.cornell.edu

In Lai & Tsang (2009), we studied the global corotational instability of non-axisymmetric p-modes (also called intertial-acoustic modes) trapped in the inner-most region of the accretion disc around a black hole. These modes do not have nodes in the vertical direction, and were shown to be amplified by the effect of wave absorption at corotation resonance. Near the black hole the radial epicyclic frequency κ reaches a maximum and goes to zero at the innermost stable circular orbit (ISCO). This causes a non-monotonic behavior in the fluid vortensity, $\zeta = \kappa^2/(2\Sigma\Omega)$, such that $d\zeta/dr > 0$ inside the radius where ζ peaks. It can be shown that the sign of the corotational wave absorption depends on the sign of the vortensity gradient $d\zeta/dr$ (Tsang & Lai 2008; see Goldreich & Tremaine 1979). Thus p-modes with positive vortensity gradient at the corotation radius can be overstable due to corotational wave absorption. Tagger & Pellat (2002) and Tagger & Varniere (2006) showed that the global p-mode intability can be enhanced when the disc is threaded by a strong (of order equipartion), large-scale poloidal magnetic field.

Our previous study (Lai & Tsang 2009) and much of the related work on disc dynamics have assumed barotropic flows for the disc (i.e. the pressure depends only on density). This assumption provides convenient simplification, but may miss important effects of the disc dynamics. For example, Lovelace et al. (1999) and Li et al. (2000) studied the adiabatic perturbations for waves trapped by a disk entropy radial profile that has a localized maximum, leading to the so-called Rossby-wave instability. They showed that in such a case the key parameter determining the effect of the corotation is no longer the gradient of the vortensity, but rather the slope of a modified effective vortensity, $\zeta_{\rm eff} \equiv \zeta/S^{2/\Gamma}$, where $S \equiv P/\Sigma^\Gamma$ is defined as the entropy and Γ is the 2-dimensional adiabatic index (assumed to be constant). As another example, Baruteau & Masset (2008) showed that the corotation torque of a protoplanetary disc on a planet can be significantly different for barotropic and non-barotropic fluids.

In this paper we study the global corotational instability of p-modes in accretion discs around black holes, generalizing our pevious works (Tsang & Lai 2008; Lai & Tsang 2009) to include non-barotropic effects. In section 2 we develop the basic equations of adiabatic perturbations for generic accretion discs. In section 3 we analyze the effect of the corotation resonance, including a careful treatment of both the first and second-order singularities of the resonance; we derive a WKB expression for the reflectivity due to the corotation barrier and show that super-reflection can be achieved under certain conditions. In section 4 we consider black hole disc models parametrized by α-viscosity, and calculate the global disc p-mode frequencies and growth rates. Finally, in section 5 we discuss the implications of this work for models of high-frequency QPOs.

2   BASIC EQUATIONS

We begin by considering the basic fluid equations of a 2-dimensional disc. The continuity and momentum equations read:

$$\partial_t \Sigma + \mathbf{u} \cdot \nabla \Sigma + \Sigma \nabla \cdot \mathbf{u} \quad = \quad 0 \ , \tag{1a}$$

$$\partial_t \mathbf{u} + (\mathbf{u} \cdot \nabla)\mathbf{u} \quad = \quad -\frac{1}{\Sigma}\nabla P - \nabla \Phi \ , \tag{1b}$$

where $P(r) = \int p\, dz$ is the vertically integrated pressure, and $\Sigma(r) = \int \rho\, dz$ is the surface density and we adopt the Pacyznski-Wiita psuedo-Newtonian potential $\Phi = GM/(r - 2r_g)$ with $r_g = GM/c^2$. Assuming that the background flow has $\mathbf{u} = r\Omega\hat{\phi}$, and that the Eulerian perturbations $\delta\Sigma$, δP, and $\delta\mathbf{u} = \delta u_r \hat{r} + \delta u_\phi \hat{\phi}$, have the form $\exp(im\phi - i\omega t)$, we find the linear perturbation equations:

$$-i\tilde{\omega}\delta\Sigma + \frac{1}{r}\frac{\partial}{\partial r}(\Sigma r \delta u_r) + \frac{im}{r}\Sigma\delta u_\phi \quad = \quad 0 \ , \tag{2a}$$

$$-i\tilde{\omega}\delta u_r - 2\Omega\delta u_\phi \quad = \quad -\frac{1}{\Sigma}\frac{\partial}{\partial r}\delta P + \frac{\delta\Sigma}{\Sigma^2}\frac{\partial P}{\partial r} \ , \tag{2b}$$

$$-i\tilde{\omega}\delta u_\phi + \frac{\kappa^2}{2\Omega}\delta u_r \quad = \quad -\frac{im}{r}\frac{\delta P}{\Sigma} \ , \tag{2c}$$

where $c_s^2 = \partial P/\partial \Sigma$ is the adiabatic sound speed, $\tilde{\omega} = \omega - m\Omega$ and κ is the radial epicyclic (angular) frequency.

Tsang & Lai (2008) and Lai & Tsang (2009) assumed the disc fluid is barotropic such that $P = P(\Sigma)$. Here we consider adiabatic perturbations of a general non-barotropic disc. The Lagrangian density perturbation $\Delta\Sigma$ and pressure perturbation ΔP are related by

$$\Delta\Sigma = \frac{1}{c_s^2}\Delta P \ . \tag{3}$$

This gives

$$\delta\Sigma \quad = \quad \frac{1}{c_s^2}\delta P + \left(\frac{1}{c_s^2}\frac{dP}{dr} - \frac{d\Sigma}{dr}\right)\xi_r = \frac{1}{c_s^2}\delta P + \frac{\Sigma^2 N_r^2}{dP/dr}\frac{i\delta u_r}{\tilde{\omega}} \tag{4}$$

where $\xi_r = i\delta u_r/\tilde{\omega}$ is the Lagrangian displacement in the r direction, and N_r is the radial Brunt-Väisäla frequency as given

by

$$N_r^2 = \frac{1}{\Sigma^2} \left(\frac{dP}{dr} \right)^2 \left(\frac{d\Sigma}{dP} - \frac{1}{c_s^2} \right) . \tag{5}$$

Combining the above with the linearized perturbation equations (2a)-(2c), and eliminating δu_ϕ, we obtain two coupled first-order ODEs appropriate for numerical integration

$$\delta h' = \left(\frac{\Sigma N_r^2}{P'} + \frac{2m\Omega}{\tilde{\omega} r} \right) \delta h + \frac{D_s}{\tilde{\omega}} i\delta u_r , \tag{6a}$$

$$i\delta u_r' = \left(\frac{m^2}{\tilde{\omega} r^2} - \frac{\tilde{\omega}}{c_s^2} \right) \delta h - \left[\frac{\Sigma N_r^2}{P'} + \frac{m\kappa^2}{2r\Omega\tilde{\omega}} + (\ln r\Sigma)' \right] i\delta u_r , \tag{6b}$$

where $\delta h = \delta P/\Sigma$ is the enthalpy perturbation, " $'$ " denotes $\partial/\partial r$ and

$$D_s \equiv \kappa^2 - \tilde{\omega}^2 + N_r^2 . \tag{7}$$

Eliminating δu_r we arrive at the second order differential equation for δh,

$$0 = \frac{\partial^2}{\partial r^2}\delta h - \frac{d}{dr}\left(\ln \frac{D_s}{r\Sigma} \right)\frac{\partial}{\partial r}\delta h - \left[\frac{m^2}{r^2} + \frac{D_s}{c_s^2} + \frac{2m\Omega}{r\tilde{\omega}}\frac{d}{dr}\left(\ln \frac{\Omega\Sigma}{D_s} \right) \right]\delta h$$
$$- \left[\left(\frac{1}{L_S} \right)^2 + \frac{d}{dr}\left(\frac{1}{L_S} \right) - \frac{1}{L_S}\frac{d}{dr}\left(\ln \frac{D_s}{r\Sigma} \right) + \frac{4m\Omega}{\tilde{\omega} r L_S} - \frac{m^2 N_r^2}{r^2 \tilde{\omega}^2} \right]\delta h . \tag{8}$$

where

$$\frac{1}{L_S} \equiv \frac{\Sigma N_r^2}{dP/dr} . \tag{9}$$

It is convenient to eliminate the term proportional to $\delta h'$ in eq. (8) by defining

$$A^2 \equiv \frac{D_s}{r\Sigma} \qquad \text{and} \qquad \eta = \frac{\delta h}{A}, \tag{10}$$

which allows us to rewrite (8) as a wave equation:

$$0 = \frac{\partial^2}{\partial r^2}\eta - \left[\frac{m^2}{r^2} + \frac{D_s}{c_s^2} + \frac{2m\Omega}{r\tilde{\omega}}\frac{d}{dr}\left(\ln \frac{\Omega\Sigma}{D_s} \right) - A\frac{d^2}{dr^2}\frac{1}{A} \right]\eta$$
$$- \left[\frac{1}{L_S^2} + \frac{d}{dr}\left(\frac{1}{L_S} \right) - \frac{1}{L_S}\frac{d}{dr}\left(\ln \frac{D_s}{r\Sigma} \right) + \frac{4m\Omega}{\tilde{\omega} r L_S} + \frac{m^2 N_r^2}{r^2 \tilde{\omega}^2} \right]\eta , \tag{11}$$

Equation (11) forms the basis of our analysis in section 3. If the adiabatic index $\Gamma \equiv \partial \ln P/\partial \ln \Sigma = c_s^2 \Sigma/P$ is constant, one can define the "entropy",

$$S \equiv P/\Sigma^\Gamma . \tag{12}$$

Then

$$N_r^2 = -\frac{1}{\Gamma\Sigma}\frac{dP}{dr}\frac{d\ln S}{dr} , \tag{13}$$

and

$$L_S^{-1} = \frac{1}{\Gamma}\frac{d\, lnS}{dr} , \tag{14}$$

and eq. (8) reduces to eq. (10) in Lovelace et al (1999). When $N_r \to 0$ (thus $L_s^{-1} \to 0$), the terms on the second line of eq. (8) vanish and we recover the second order perturbation equation for barotropic flows (Goldreich & Tremaine 1979; Tsang & Lai 2008).

3   REFLECTION OF THE COROTATION BARRIER

Away from the corotation resonance (where $\tilde{\omega} = 0$) region, eq. (11) yields local WKB wave solution $\delta h \propto \exp(i \int k_r dr)$, with $D_s/c_s^2 \simeq -k_r^2$, or

$$\tilde{\omega}^2 \simeq \kappa^2 + N_r^2 + k_r^2 c_s^2. \tag{15}$$

Since typically $N_r^2 \lesssim c_s^2/r^2 \ll \kappa^2 \sim \Omega^2$ (for thin discs), this is the standard dispersion relation for spiral density waves. The inner/outer Lindblad resonances (I/OLR) are defined by $\tilde{\omega} = \pm\sqrt{\kappa^2 + N_r^2} \simeq \pm\kappa$. Waves can propagate inside the ILR ($r < r_{\rm IL}$) or outside the OLR ($r > r_{\rm OL}$). between $r_{\rm IL}$ and $r_{\rm OL}$ lies the corotation barrier.

In this section, we derive the expression for the (complex) reflection coefficient for waves incident upon the corotation barrier and deduce the condition for super-reflection. Our analysis generalizes that given in Tsang & Lai (2008), which assumed barotropic fluids.

3.1 Analytical Calculation of the Reflectivity

Near the corotation resonance $r = r_c$ where $\tilde{\omega} = 0$, we can rewrite eq. (11) as

$$\left[\frac{d^2}{dr^2} - k_{\text{eff}}^2 + \frac{2}{q} \left(\frac{d}{dr} \ln \frac{\kappa^2}{\Omega\Sigma} - \frac{2}{L_S} \right) \frac{1}{r - R_c} - \frac{N_r^2}{q^2\Omega^2} \frac{1}{(r - R_c)^2} \right] \eta = 0 , \tag{16}$$

where $q \equiv -(d\ln\Omega/d\ln r)_c$, $R_c \equiv r_c - i\frac{r_c\omega_i}{q\omega_r}$, and k_{eff} given by

$$-k_{\text{eff}}^2 \equiv \frac{m^2}{r^2} + \frac{D_s}{c_s^2} - A\frac{d^2}{dr^2}\frac{1}{A} + \frac{1}{L_S^2} + \frac{d}{dr}\left(\frac{1}{L_S}\right) - \frac{1}{L_S}\frac{d}{dr}\left(\ln\frac{D_s}{r\Sigma}\right) , \tag{17}$$

is the effective radial wave number without the terms singular at the corotation. We have introduced a small imaginary part to the wave frequency so that $\omega = \omega_r + i\omega_i$ (with $\omega_i > 0$). Defining

$$x \equiv \int_{r_c}^{r} 2k_{\text{eff}}dr, \qquad \psi \equiv \sqrt{k_{\text{eff}}}\eta, \qquad \text{and } \epsilon \equiv \frac{2k_{\text{eff}}r_c}{q}\frac{\omega_i}{\omega_r} , \tag{18}$$

we have

$$\frac{d^2}{dx^2}\psi + \left[-\frac{1}{4} + \frac{\nu}{x + i\epsilon} + \frac{\frac{1}{4} - \mu^2}{(x + i\epsilon)^2} \right] \psi = 0 , \tag{19}$$

which we recognize as the Whittaker differential equation (Abramowitz & Stegun 1964). In eq. (19) we have defined

$$\nu = \left[\frac{c_s}{q\kappa} \left(\frac{d}{dr} \ln\zeta - \frac{2}{L_S} \right) \right]_c , \tag{20}$$

$$\mu = \frac{1}{2}\left(1 - \frac{4N_r^2}{q^2\Omega^2} \right)_c^{1/2} , \tag{21}$$

where

$$\zeta \equiv \frac{\kappa^2}{2\Omega\Sigma} \tag{22}$$

is the vortensity for the background flow. When the adiabatic index $\Gamma = $ constant. we can use eq. (14) for L_S^{-1}, and define the effective vortensity ζ_{eff} so that

$$\nu = \left(\frac{c_s}{q\kappa}\frac{d}{dr}\ln\zeta_{\text{eff}} \right)_c , \tag{23}$$

with

$$\zeta_{\text{eff}} \equiv \frac{\kappa^2}{2\Omega\Sigma S^{2/\Gamma}} . \tag{24}$$

Typically $\kappa \sim \Omega$ (away from the ISCO) and $|N_r| \lesssim c_s/r \ll \Omega$ (for thin discs), and we have in order of magnitude $|\nu| \sim c_s/(r\Omega)$ and $|\mu - \frac{1}{2}| \sim N_r^2/c_s^2 \lesssim c_s^2/(r\Omega)^2$.

Equation (19) is solved by the Whittaker functions with indices ν and μ. The two linearly independent functions of $z = x + i\epsilon$ convenient for construction of connection coefficients are

$$\psi_- = W_{\nu,\mu}(z), \qquad \text{and} \qquad \psi_+ = e^{-i\pi\nu}W_{-\nu,\mu}(ze^{-i\pi}) + \frac{1}{2}T_0 W_{\nu,\mu}(z), \tag{25}$$

where T_0 is the stokes multiplier (defined below), and z is defined such that $\arg(z)$ ranges from 0 to π. The resulting connection formulae (Tsang & Lai 2008) are:

$$\delta h_- \sim \begin{cases} \frac{A}{\sqrt{k_{\text{eff}}}}\exp\left(-\int_{r_c}^{r}k_{\text{eff}}\,dr\right) & \text{for } r \gg r_c \\ \frac{A}{\sqrt{k_{\text{eff}}}}e^{i\pi\nu}\exp\left(+\int_{r}^{r_c}k_{\text{eff}}\,dr\right) + \frac{A}{\sqrt{k_{\text{eff}}}}\frac{T_1}{2}e^{-i\pi\nu}\exp\left(-\int_{r}^{r_c}k_{\text{eff}}\,dr\right) & \text{for } r \ll r_c . \end{cases} \tag{26}$$

$$\delta h_+ \sim \begin{cases} \frac{A}{\sqrt{k_{\text{eff}}}}\exp\left(+\int_{r_c}^{r}k_{\text{eff}}\,dr\right) & \text{for } r \gg r_c \\ \frac{A}{\sqrt{k_{\text{eff}}}}\frac{T_0}{2}e^{i\pi\nu}\exp\left(+\int_{r}^{r_c}k_{\text{eff}}\,dr\right) + \frac{A}{\sqrt{k_{\text{eff}}}}\left(1 + \frac{T_1 T_0}{4}\right)e^{-i\pi\nu}\exp\left(-\int_{r}^{r_c}k_{\text{eff}}\,dr\right) & \text{for } r \ll r_c \end{cases} \tag{27}$$

where the Stokes multipliers (Heading 1962) are given by

$$T_0 = \frac{2\pi i}{\Gamma(\frac{1}{2} - \mu + \nu)\Gamma(\frac{1}{2} + \mu + \nu)}, \qquad T_1 = \frac{2\pi i\,e^{i2\pi\nu}}{\Gamma(\frac{1}{2} - \mu - \nu)\Gamma(\frac{1}{2} + \mu - \nu)}. \tag{28}$$

The connection formulae (26)-(27) here are the same as eqs. (42)-(43) of Tsang & Lai (2008), the differences lie in the expressions for ν [eq. (20)], T_0 and T_1 [eq. (28)]. For barotropic fluids, $L_S \to \infty$ and $N_r^2 \to 0$ (and thus $\mu \to 1/2$), our expressions reduce to those given in Tsang & Lai (2008). Using the connection formulae (26)-(27) and the connection formulae for the Lindblad resonances given by eqs. (32)-(35) in Tsang & Lai (2008), we can obtain the reflection and transmission

coefficients for waves incident upon the corotation barrier for $r < r_{\mathrm{IL}}$:

$$\mathcal{R} = \frac{1 + \frac{1}{4}e^{-i2\pi\nu}e^{-2\Theta_{\mathrm{II}}}\left(1 + \frac{1}{4}T_0 T_1\right) + \frac{i}{4}T_1 e^{-i2\pi\nu}e^{-2\Theta_{\mathrm{IIa}}} - \frac{i}{4}T_0 e^{-2\Theta_{\mathrm{IIb}}}}{1 - \frac{1}{4}e^{-i2\pi\nu}e^{-2\Theta_{\mathrm{II}}}\left(1 + \frac{1}{4}T_0 T_1\right) - \frac{i}{4}T_1 e^{-i2\pi\nu}e^{-2\Theta_{\mathrm{IIa}}} - \frac{i}{4}T_0 e^{-2\Theta_{\mathrm{IIb}}}} , \tag{29}$$

$$\mathcal{T} = \frac{-i\, e^{-\Theta_{\mathrm{II}}}e^{i\pi\nu}}{1 - \frac{1}{4}e^{-i2\pi\nu}e^{-2\Theta_{\mathrm{II}}}\left(1 + \frac{1}{4}T_0 T_1\right) - \frac{i}{4}T_1 e^{-i2\pi\nu}e^{-2\Theta_{\mathrm{IIa}}} - \frac{i}{4}T_0 e^{-2\Theta_{\mathrm{IIb}}}} , \tag{30}$$

where

$$\Theta_{\mathrm{II}} = \int_{r_{\mathrm{IL}}}^{r_{\mathrm{OL}}} \sqrt{-k_{\mathrm{eff}}^2}\, dr, \qquad \Theta_{\mathrm{IIa}} = \int_{r_{\mathrm{IL}}}^{r_c} \sqrt{-k_{\mathrm{eff}}^2}\, dr, \text{ and} \qquad \Theta_{\mathrm{IIb}} = \int_{r_c}^{r_{\mathrm{OL}}} \sqrt{-k_{\mathrm{eff}}^2}\, dr. \tag{31}$$

For $|\nu| \ll 1$ and $|\mu - \frac{1}{2}| \ll 1$ eq. (29) can be simplified to

$$\mathcal{R} = \frac{e^{\Theta_{\mathrm{II}}} + \frac{1}{4}e^{-\Theta_{\mathrm{II}}}}{e^{\Theta_{\mathrm{II}}} - \frac{1}{4}e^{-\Theta_{\mathrm{II}}}} + \frac{e^{+2\Theta_{\mathrm{IIb}}} + i - \frac{1}{4}e^{-2\Theta_{\mathrm{IIb}}}}{\left(e^{\Theta_{\mathrm{II}}} - \frac{1}{4}e^{-\Theta_{\mathrm{II}}}\right)^2}\pi\nu + \frac{e^{+2\Theta_{\mathrm{IIb}}} - \frac{1}{4}e^{-2\Theta_{\mathrm{IIb}}}}{\left(e^{\Theta_{\mathrm{II}}} - \frac{1}{4}e^{-\Theta_{\mathrm{II}}}\right)^2}\pi(\mu - \tfrac{1}{2}) + \mathcal{O}[\nu^2, (\mu - \tfrac{1}{2})^2] . \tag{32}$$

For $\Theta_{\mathrm{IIb}} \gg 1$ and $\Theta_{\mathrm{IIa}} \gg 1$ this further reduces to

$$\mathcal{R} - 1 \simeq \left(\nu + \mu - \frac{1}{2}\right)\pi e^{-2\Theta_{\mathrm{IIa}}} . \tag{33}$$

Thus, super-reflection occurs when $\nu + \mu + \frac{1}{2} \simeq \nu > 0$ [since $|\mu - \frac{1}{2}|$ is much smaller than $|\nu|$; see eqs (20) - (21)] .

3.2 Numerical Calculation of Reflectivity

We can also calculate the reflectivity numerically by integrating eqs. (6a) - (6b). To this end, we assume an outgoing wave at some radius $r_{\mathrm{out}} \gg r_{\mathrm{OL}}$, motivated by the wave equation (11):

$$\delta h \propto \frac{A}{\sqrt{k_r}}\exp\left[i\int_{r_{\mathrm{OL}}}^{r} k_r dr + i\frac{\pi}{4}\right] . \tag{34}$$

where k_r is the full radial wave-number given by

$$-k_r^2 \equiv \frac{m^2}{r^2} + \frac{D_s}{c_s^2} + \frac{2m\Omega}{r\tilde{\omega}}\frac{d}{dr}\left(\ln\frac{\Omega\Sigma}{D_s}\right) - A\frac{d^2}{dr^2}\frac{1}{A} + \frac{1}{L_S^2} + \frac{d}{dr}\left(\frac{1}{L_S}\right) - \frac{1}{L_S}\frac{d}{dr}\left(\ln\frac{D_s}{r\Sigma}\right) + \frac{4m\Omega}{\tilde{\omega}rL_S} + \frac{m^2 N_r^2}{r^2\tilde{\omega}^2} . \tag{35}$$

This gives the outer boundary condition at $r = r_{\mathrm{out}}$

$$\delta h'(r_{\mathrm{out}}) = \left(ik_r + \frac{d}{dr}\ln A - \frac{1}{2}\frac{d}{dr}\ln k_r\right)\delta h(r_{\mathrm{out}}) . \tag{36}$$

At some inner radius $r_{\mathrm{in}} \ll r_{\mathrm{IL}}$, the solution takes the form

$$\delta h \propto \frac{A}{\sqrt{k_r}}\left(\exp\left[i\int_{r}^{r_{\mathrm{IL}}} k_r\, dr + i\frac{\pi}{4}\right] + \mathcal{R}\exp\left[-i\int_{r}^{r_{\mathrm{IL}}} k_r\, dr - i\frac{\pi}{4}\right]\right) , \tag{37}$$

and the reflection coefficient can be obtained from

$$|\mathcal{R}| = \left|\frac{\left(\frac{d}{dr}\ln A - \frac{1}{2}\frac{d}{dr}\ln k_r - ik_r\right)\delta h - \delta h'}{\left(\frac{d}{dr}\ln A - \frac{1}{2}\frac{d}{dr}\ln k_r + ik_r\right)\delta h - \delta h'}\right|_{r_{\mathrm{in}}} . \tag{38}$$

Fig. 1 gives some examples of the reflectivity for a simple power-law disc model. We parameterize the relevant disc profiles by assuming $\Sigma \propto r^{-p}$, $N_r^2 = N_c^2(r/r_c)^{-b}$ and $L_S = L_{Sc}(r/r_c)^{-\gamma}$, and we fix the sound speed to $c_s/(r\Omega) = 0.1$. Note that for non-barotropic fluids $P \neq \Sigma c_s^2$, thus we allow N_r^2 and $L_S^{-1} = \Sigma N_r^2/P'$ to vary independently. In the examples depicted in Fig. 1, we fix $N_r(r)$ and $L_S(r)$, but vary the density index, p, to change the critical parameter ν [see eq. (20)]. In general, as seen from eqs. (6a) - (6b) or eq. (11), the result depends on N_c, L_{Sc}, b, and γ, but we find that the dependence on b and γ to be rather weak. In agreement with the analytic expression in Section 3.1 [eq. (33)], we find that the super-reflection ($|\mathcal{R}| > 1$) is achieved when $\nu + \mu - \frac{1}{2} \simeq \nu > 0$.

4 CALCULATION OF GLOBAL OVERSTABLE P-MODES IN BLACK HOLE ACCRETION DISCS

The result of Section 3 shows that when $\nu + \mu - \frac{1}{2} > 0$, waves impinging upon the corotation barrier are super-reflected. Supposing there exists a reflecting boundary at the inner disc radius $r_{\mathrm{in}} = r_{\mathrm{ISCO}}$, normal p-modes can be produced, with waves trapped between r_{in} and r_{IL}. In the WKB approximation the mode growth rate ω_i is directly related to the reflectivity $|\mathcal{R}|$ (Tsang & Lai 2008)

$$\omega_i \simeq \left(\frac{|\mathcal{R}| - 1}{|\mathcal{R}| + 1}\right)\left[\int_{r_{\mathrm{in}}}^{r_{\mathrm{IL}}}\frac{|\tilde{\omega}_r|}{c_s\sqrt{\tilde{\omega}_r^2 - \kappa^2}}dr\right]^{-1} \tag{39}$$

where $\tilde{\omega}_r = \mathrm{Re}(\omega) - m\Omega$. More accurate calculation of the p-mode frequency $\omega = \omega_r + i\omega_i$ requires solving the complex eigenvalue problem based on eqs. (6a) - (6b).
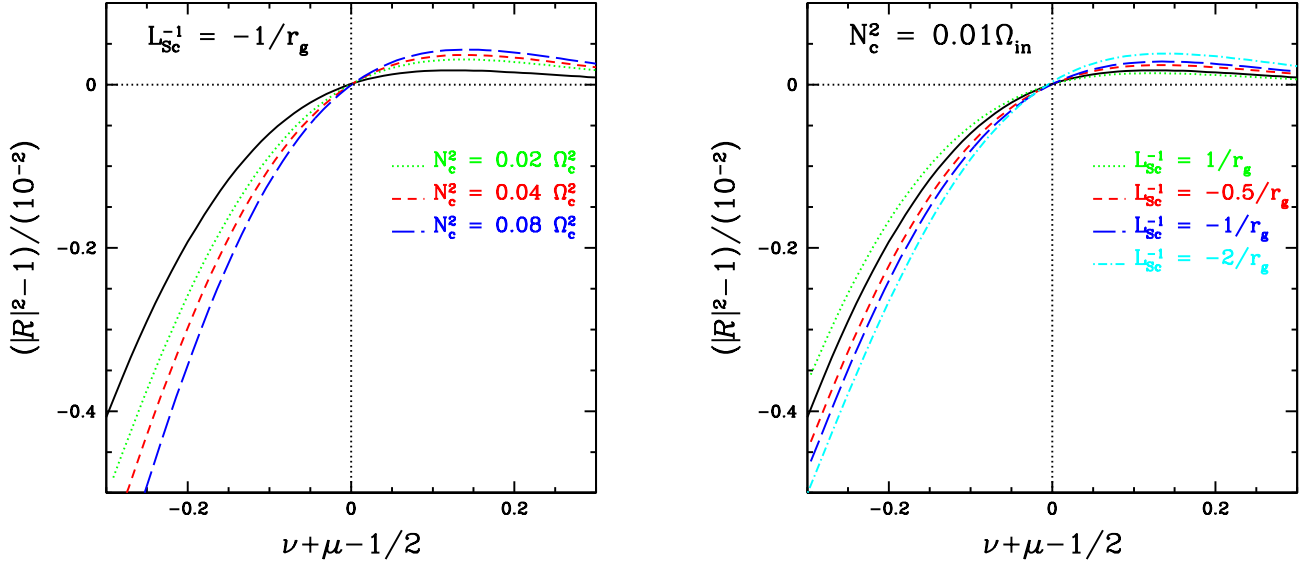
Figure 1. Reflectivity of the corotation barrier in a Keplerian disc. The disc background profiles are given by $\Omega \propto r^{-3/2}$, $L_S = L_{Sc}(r/r_c)^{-1}$, $N_r^2 = N_c^2(r/r_c)^{-3/2}$, and the sound speed given by $c_s/(r_c\Omega_c) = 0.1$. The horizontal axis gives $\nu + \mu - \frac{1}{2}$ [see eqs. (32) - (33)]. The parameter ν is varied by changing the density profile $\Sigma \propto (r/r_c)^{-p}$. The reflectivity for barotropic fluids (Tsang & Lai 2008) is recovered for $N_c^2 = 0$ and $L_{Sc}^{-1} = 0$, shown as the solid line.

4.1   Background Disk Structure

As an illustration of the global p-mode calculation, we consider the standard α-disc model. For the inner region of the disc we are most concerned with, radiation pressure dominates gas pressure, and the opacity is primarily due to electron scattering. However it is well known that with the standard viscosity prescription for the viscous stress tensor $\sigma_{r\phi} = -\alpha P_{\text{total}}$, this inner disc solution is thermally unstable (Shakura & Sunyaev 1976). We therefore also consider a slightly modified disk model where $\sigma_{r\phi} = -\alpha P_{\text{gas}}$ is adopted – this disc solution is thermally stable in the inner region (Lightman 1974). Consistent with our perturbation analysis, we use the Paczynski-Wiita potential $\Phi = -GM/(r - 2r_g)$ (where $r_g = GM/c^2$) to mimic the general relativistic effect (Paczynski & Wiita 1980).

With the viscosity prescription $\sigma_{r\phi} = -\alpha P_{\text{total}}$ the relevant background disk profiles are

$$\Sigma(r) = (6.95 \text{ g cm}^{-2})M_{10}\dot{M}_{18}^{-1}\alpha^{-1}\left(\frac{r}{r_g}\right)^{3/2}\left(1 - \frac{2r_g}{r}\right)^3\left(1 - \frac{2r_g}{3r}\right)^{-2}\mathcal{J}^{-1} \tag{40a}$$

$$P(r) = (3.24 \times 10^{21} \text{ erg cm}^{-2})M_{10}^{-1}\dot{M}_{18}^{-1}\alpha^{-1}\left(\frac{r}{r_g}\right)^{-3/2}\left(1 - \frac{2r_g}{r}\right)^{-1}\mathcal{J} \tag{40b}$$

$$H(r) = (1.06 \times 10^6 \text{ cm})\dot{M}_{18}\left(1 - \frac{2r_g}{r}\right)^{-1}\left(1 - \frac{2r_g}{3r}\right)\mathcal{J} . \tag{40c}$$

where $M_{10} = M/(10M_\odot)$, $\dot{M} = (10^{18}gs^{-1})\dot{M}_{18}$ is the accretion rate, $H(r)$ is the vertical scale height, and $\mathcal{J} \equiv 1 - l_o/l(r)$ with $l(r) = \Omega r^2$. The constant l_o specifies the specific angular momentum absorbed at the inner edge of the disc per unit accreting mass; one typically expects $l_o \leqslant l(r_{\text{in}})$ [$l_o = l(r_{\text{in}})$ is the so-called zero-torque condition].

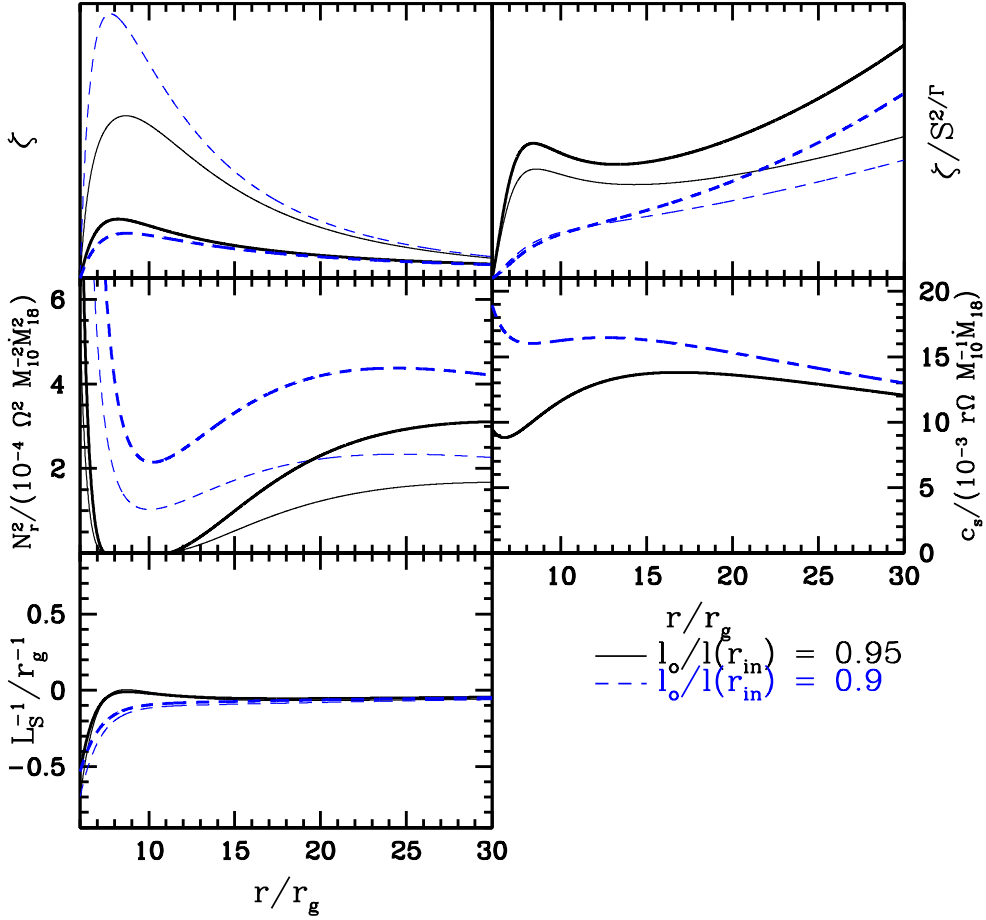The viscosity prescription with $\sigma_{r\phi} = -\alpha P_{\text{gas}}$ yields

$$\Sigma(r) = (7.02 \times 10^4 \text{ g cm}^{-2})M_{10}^{-\frac{2}{5}}\dot{M}_{18}^{\frac{3}{5}}\alpha^{-\frac{4}{5}}\left(\frac{r}{r_g}\right)^{-\frac{3}{5}}\left(1 - \frac{2r_g}{r}\right)^{-\frac{1}{5}}\left(1 - \frac{2r_g}{3r}\right)^{-\frac{1}{5}}\mathcal{J}^{\frac{3}{5}} , \tag{41a}$$

$$P(r) = (3.27 \times 10^{25} \text{ erg cm}^{-2})M_{10}^{-\frac{12}{5}}\dot{M}_{18}^{\frac{13}{5}}\alpha^{-\frac{4}{5}}\left(\frac{r}{r_g}\right)^{-\frac{18}{5}}\left(1 - \frac{2r_g}{r}\right)^{-\frac{21}{5}}\left(1 - \frac{2r_g}{3r}\right)^{\frac{9}{5}}\mathcal{J}^{\frac{13}{5}} , \tag{41b}$$

$$H(r) = (1.06 \times 10^6 \text{ cm})\dot{M}_{18}\left(1 - \frac{2r_g}{r}\right)^{-1}\left(1 - \frac{2r_g}{3r}\right)\mathcal{J} . \tag{41c}$$

In both cases we obtain the 2-dimensional adiabatic sound speed by $c_s^2 = \Gamma P/\Sigma$, giving

$$\frac{c_s}{r\Omega} = 0.72\Gamma^{1/2}M_{10}^{-1}\dot{M}_{18}\left(\frac{r}{r_g}\right)^{-1}\left(1 - \frac{2r_g}{3r}\right)\left(1 - \frac{2r_g}{r}\right)^{-1}\mathcal{J} . \tag{42}$$

Figure 2. The background disc solutions for α-disc models. The depicted profiles are: the vortensity $\zeta = \kappa^2/(2\Sigma\Omega)$ and the modified vortensity $\zeta_{\rm eff} = \zeta/S^{2/\Gamma}$ [both in arbitrary units; see eqs. (22) and (24)]; the squared radial Brunt-Väisäla frequency N_r^2, the inverse entropy length-scale L_S^{-1} [see eqs.(12) - (14)], and the sound speed c_s. The adiabatic index is assumed to be $\Gamma = 1.4$. The solid and dashed lines denote different angular momentum eigenvalues l_o. The thick lines show the profiles for the $\sigma_{r\phi} = -\alpha P_{\rm gas}$ prescription, while the thin lines show the profiles for the $\sigma_{r\phi} = -\alpha P_{\rm total}$ prescription.

For simplicity, we adopt $\Gamma = 1.4$ in our calculations (using somewhat different values do not affect our results in Section 4.2). Fig. 2 depicts the disc background profiles important for our p-mode calculations.

4.2 Growing Eigenmodes

In addition to the outgoing boundary condition (36) at some $r_{\rm out} \gg r_{\rm OL}$, it is necessary to impose an appropriate inner boundary condition (at $r_{\rm in} = r_{\rm ISCO}$) in order to calculate the global p-modes trapped between $r_{\rm in}$ and $r_{\rm IL}$. Unfortunately this inner boundary condition is uncertain: the large radial velocity of the transonic flow around $r_{\rm ISCO}$ leads to energy loss of the wave, while the sharp density gradient at $r_{\rm ISCO}$ provides a partially reflecting inner boundary (see Lai & Tsang 2009); in real black-hole accretion flows, a large magnetic flux accumulation inside $r_{\rm ISCO}$ can make the inner disc edge an even better reflector for waves. Here, to focus on the role of the corotational instability, we adopt the free boundary condition (zero Lagrangian pressure perturbation) at $r_{\rm in} = r_{\rm ISCO}$, i.e.

$$\Delta P = \left(\delta P + \frac{dP}{dr} \frac{i\delta u_r}{\tilde{\omega}} \right)_{r_{\rm in}} = 0 \ . \tag{43}$$

With eq. (36) and eq. (43) we employ the standard shooting method (Press et. al 1995) with eqs. (6a) and (6b), to solve for the eigenvalue $\omega = \omega_r + i\omega_i$. Table 1 summarizes the results for different background disc parameters, and example wavefunctions for the zero and one-node eigenmodes are shown in Fig. 3. We see that the trapping region extends from the inner edge of the disc at $r_{\rm ISCO}$ to the inner Lindblad resonance $r_{\rm IL}$. The wave is evanescent in the corotation barrier region
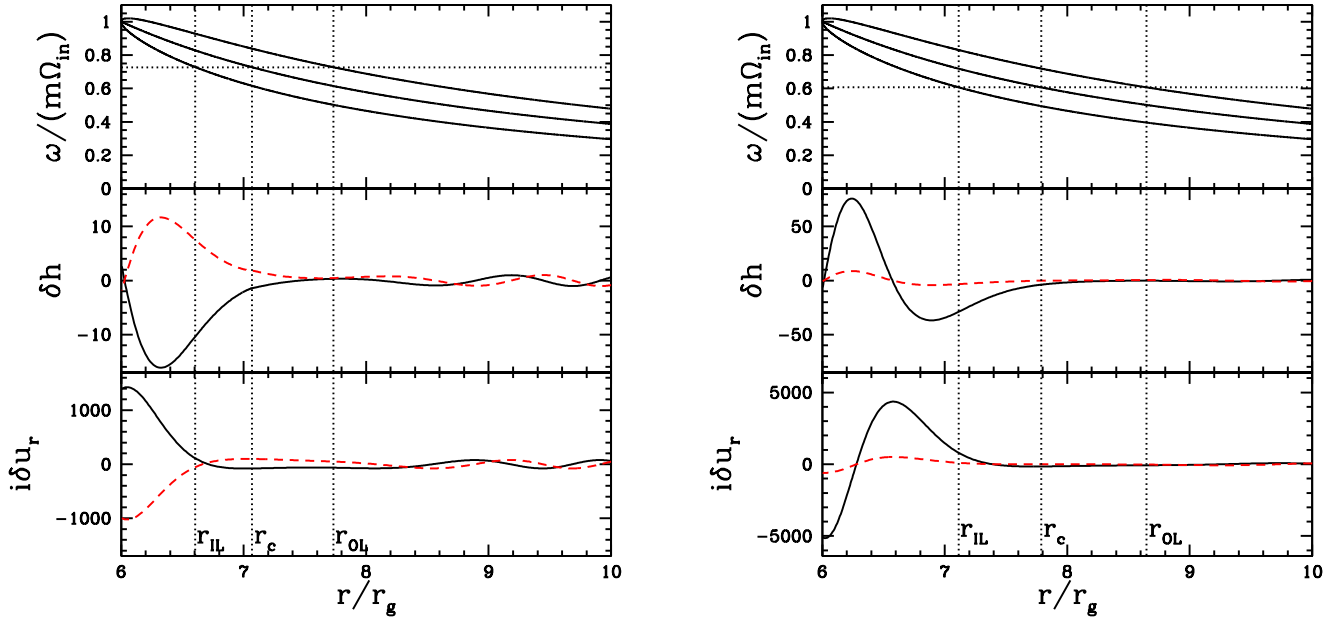
Figure 3. Eigenunctions of disc p-modes with $m = 3$. The disc model parameters are $\dot{M}_{18} = 3$, and $l_o/l(r_{\rm in}) = 0.95$, with the viscous stress tensor given by $\sigma_{r\phi} = -\alpha P_{\rm gas}$. The left panel shows the propagation diagram and eigenfunctions for the zero-node (in the trapping region) mode, with eigenfrequency of $\omega/\Omega_{\rm in} = 2.18 + i3.0 \times 10^{-3}$. The right plot shows the propagation diagram and eigenfunctions the single-node mode with $\omega/\Omega_{\rm in} = 1.82 + i2.3 \times 10^{-4}$. For the eigenfunctions, the solid lines denote the real parts, while the dashed lines denote the imaginary parts.

between $r_{\rm IL}$ and $r_{\rm OL}$, and tunnels out to the propagation region ($r > r_{\rm OL}$). In the following we will focus on the 0-node modes since they have growth rates much larger than the 1-node modes.

From Table 1 we see that for a given disc model, the (real) mode pattern freqency ω_r/m increases only slightly as m increases, while the growth rate more rapidly increases with increasing m. In particular, the $m = 1$ mode has a much smaller growth rate than the higher-m modes. These features can be easily understood by examining the propagation diagram (Fig. 4). For small m, the wave trapping region between $r_{\rm ISCO}$ and $r_{\rm IL}$ is slimmer, thus to "contain" the same number of wavelengths in the trapping region, the pattern frequency must be lower. On the other hand, the wider corotation barrier for small m implies that only a small amount of wave energy can tunnel through the barrier, giving rise to smaller corotational wave absorption and a slow mode growth rate. As can be seen from Fig. 4, the difference in the width of the evanescent regions is greatest between the $m = 1$ and $m = 2$; the lower pattern frequency of lower m modes also helps to widen the evanescent region. These explain why the $m = 1$ mode has such a small growth rate compared to the other modes.

Table 1 shows that for the α-disc models considered, the mode frequency decreases slightly as $\dot{M}$ increases (while keeping the other disc parameters fixed). This results from the increase of the disc sound speed c_s [see eq. (42)]. Table 1 also shows that the $m = 2$ and $m = 3$ modes in each disc model have roughly 2:3 commensurate frequencies, ranging from $\omega_{m=3}/\omega_{m=2} \simeq 1.57$ to 1.69 for the disc background models considered. This has implications for the observations of high-frequency QPOs (see section 5).

Fig. 5 shows the propagation diagram of $m = 2$ modes and the effective vortensity gradient profiles for both viscosity-law ($\sigma_{r\phi} = -\alpha P_{\rm total}$ vs $\sigma_{r\phi} = -\alpha P_{\rm gas}$) background disc models, with $\dot{M}_{18} = 3$, $l_o/l(r_{\rm in}) = 0.95$ and $\Gamma = 1.4$. The zero-node modes for both models occur at $\mathrm{Re}(\omega) \simeq 1.34\Omega_{\rm in}$, which has a positive effective vortensity slope at the corotation radius. However only the disc model with the $\sigma_{r\phi} = -\alpha P_{\rm total}$ prescription has a growing 1-node mode at $\mathrm{Re}(\omega) \simeq 1.04\Omega_{\rm in}$ (see Table 1). For the disc model with the $\sigma_{r\phi} = -\alpha P_{\rm gas}$ prescription, such a (real) frequency would give negative effective vortensity gradient at r_c, thus the corotation acts to damp the mode (see the inset of Fig. 5).

Overall, our numerical calculation of the global disc p-modes is in agreement with our analysis given in Section 3, i.e., wave absorption at the corotation resonance gives rise to growing p-modes when the gradient of the effective vortensity is positive at corotation.

Table 1. Overstable p-mode frequencies for various disc models.

		Mode Eigenfrequencies ($\omega/\Omega_{\rm in}$) for $\sigma_{r\phi} = -\alpha P_{\rm total}$			
	mode	$\beta = 0.9$, $\dot{M}_{18} = 1$	$\beta = 0.9$, $\dot{M}_{18} = 3$	$\beta = 0.95$, $\dot{M}_{18} = 1$	$\beta = 0.95$, $\dot{M}_{18} = 3$
$m = 1$	0-node	$0.59 + i2.2 \times 10^{-7}$	$0.39 + i4.0 \times 10^{-6}$	$0.68 + i2.2 \times 10^{-8}$	$0.52 + i1.4 \times 10^{-7}$
	1-node	$0.37 + i2.4 \times 10^{-9}$	$0.17 + i3.1 \times 10^{-9}$	–	–
$m = 2$	0-node	$1.46 + i4.0 \times 10^{-4}$	$1.13 + i1.3 \times 10^{-3}$	$1.60 + i1.2 \times 10^{-4}$	$1.35 + i6.2 \times 10^{-4}$
	1-node	$1.18 + i4.2 \times 10^{-6}$	$0.80 + i5.6 \times 10^{-5}$	$1.37 + i5.5 \times 10^{-7}$	$1.04 + i2.5 \times 10^{-6}$
$m = 3$	0-node	$2.34 + i2.6 \times 10^{-3}$	$1.91 + i5.5 \times 10^{-3}$	$2.52 + i1.2 \times 10^{-3}$	$2.20 + i3.4 \times 10^{-3}$
	1-node	$2.01 + i1.8 \times 10^{-4}$	$1.48 + i7.7 \times 10^{-4}$	$2.25 + i4.4 \times 10^{-5}$	$1.83 + i2.6 \times 10^{-4}$
$m = 4$	0-node	$3.23 + i6.0 \times 10^{-3}$	$2.71 + i1.0 \times 10^{-2}$	$3.44 + i3.2 \times 10^{-3}$	$3.06 + i7.3 \times 10^{-3}$
	1-node	$2.86 + i9.0 \times 10^{-4}$	$2.20 + i2.4 \times 10^{-3}$	$3.15 + i3.2 \times 10^{-4}$	$2.63 + i1.2 \times 10^{-3}$

		Mode Eigenfrequencies ($\omega/\Omega_{\rm in}$) for $\sigma_{r\phi} = -\alpha P_{\rm gas}$			
	mode	$\beta = 0.9$, $\dot{M}_{18} = 1$	$\beta = 0.9$, $\dot{M}_{18} = 3$	$\beta = 0.95$, $\dot{M}_{18} = 1$	$\beta = 0.95$, $\dot{M}_{18} = 3$
$m = 1$	0-node	$0.58 + i1.1 \times 10^{-7}$	$0.37 + i2.3 \times 10^{-6}$	$0.67 + i2.3 \times 10^{-8}$	–
	1-node	$0.37 + i9.6 \times 10^{-10}$	$0.16 + i1.1 \times 10^{-9}$	–	–
$m = 2$	0-node	$1.44 + i3.6 \times 10^{-4}$	$1.11 + i1.1 \times 10^{-3}$	$1.59 + i1.0 \times 10^{-4}$	$1.33 + i4.9 \times 10^{-4}$
	1-node	$1.18 + i4.2 \times 10^{-6}$	$0.79 + i6.0 \times 10^{-5}$	$1.36 + i4.3 \times 10^{-7}$	–
$m = 3$	0-node	$2.32 + i2.4 \times 10^{-3}$	$1.88 + i5.1 \times 10^{-3}$	$2.51 + i1.1 \times 10^{-3}$	$2.18 + i3.0 \times 10^{-3}$
	1-node	$2.00 + i1.9 \times 10^{-4}$	$1.47 + i8.1 \times 10^{-4}$	$2.25 + i4.4 \times 10^{-5}$	$1.82 + i2.3 \times 10^{-4}$
$m = 4$	0-node	$3.21 + i5.7 \times 10^{-3}$	$2.68 + i1.0 \times 10^{-2}$	$3.44 + i3.1 \times 10^{-3}$	$3.04 + i6.8 \times 10^{-3}$
	1-node	$2.85 + i9.3 \times 10^{-4}$	$2.19 + i2.5 \times 10^{-3}$	$3.14 + i3.2 \times 10^{-4}$	$2.62 + i1.2 \times 10^{-3}$

A dash indicates that no growing eigenmode could be found, and that the mode is damped. Here the parameter $\beta \equiv l_o/l(r_{\rm in})$ determines the inner torque condition for the background disc. The mode frequencies are independent of the value of the viscosity parameter, α, used.

5 DISCUSSION

We have studied the effect of corotation resonance on the adiabatic diskoseismic p-modes (inertial-acoustic oscillations) of non-barotropic accretion flows around black holes. Our WKB analysis of the reflectivity of the corotation barrier (Section 3), as well as our numerical calculation of the global disc p-modes (Section 4), show that the corotational wave absorption can be significantly modified by the non-barotropic effect. In particular, we have showed that super-reflection is achieved when [see eq. (33) and Fig. 1]

$$\nu + \mu - \frac{1}{2} > 0, \tag{44}$$

where ν, μ are defined by eqs. (20)-(21). For thin discs, $|\mu - 1/2| \ll 1$ and this condition is simply $\nu > 0$, or

$$\frac{d}{dr} \ln \zeta - \frac{2\Sigma N_r^2}{dP/dr} = \frac{d}{dr} \ln \left(\frac{\zeta}{S^{2/\Gamma}} \right) > 0, \tag{45}$$

where $\zeta = \kappa^2/(2\Omega\Sigma)$ is the disc vortensity, N_r is the radial Brunt-Väsälä frequency, and the first equality holds only when the adiabatic index $\Gamma = $ constant (in which case $S = P/\Sigma^\Gamma$). Thus, in the presence of a reflecting (or partially reflecting) boundary at the disc inner edge ($r = r_{\rm in}$), the non-axisymmetric p-modes trapped between $r_{\rm in}$ and the inner Lindblad resonance radius $r_{\rm IL}$ can grow due to corotational wave absorption, when the effective vortensity, $\zeta_{\rm eff} = \zeta/S^{2/\Gamma}$, has a positive slope at the corotation radius. As in the case of barotropic discs (Tsang & Lai 2008; Lai & Tsang 2009), the general relativistic effect, where κ^2 is non-monotonic and becomes smaller as r decreases toward $r_{\rm ISCO}$, plays a crucial role in the instability. Now for non-barotropic discs, the entropy gradient also plays an important role (cf. Lovelace et al. 1999).

Our calculations of the global p-modes for various disc models (see Table 1) indicate that the $m = 3$ and $m = 2$ modes (of lowest radial order) have frequency ratio in the range of 1.57–1.69, similar to the approximate 3:2 ratio as observed in high-frequency QPOs of black-hole X-ray binaries (Remillard & McClintock 2006). The growth rates for these modes are significantly higher than for the corresponding barotropic case (see Lai & Tsang 2009), due to the effect of the entropy in the effective vortensity. Although higher-m modes may grow slightly faster, they would be less likely to be observed due to averaging out of the luminosity variation over the observable emitting area. The $m = 1$ mode is found to have a significantly smaller growth rate than the $m > 1$ modes.

For our simple α-disc models, we find that the p-mode frequencies decrease slightly (by about 10-20%) as the mass
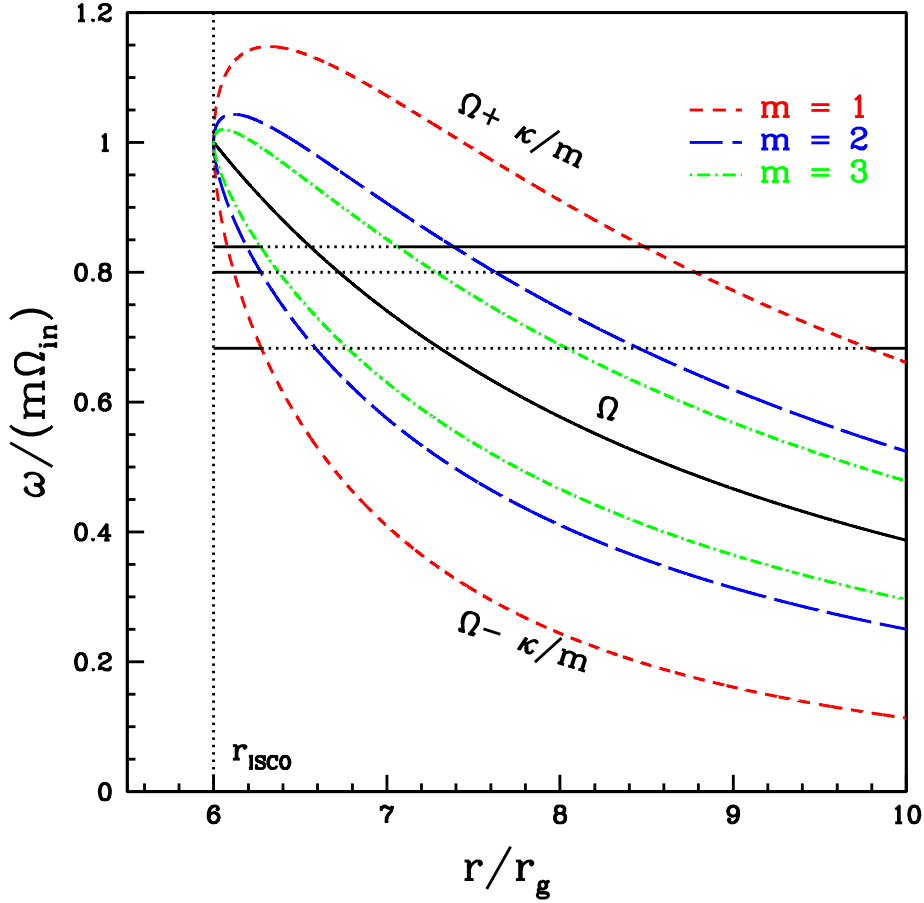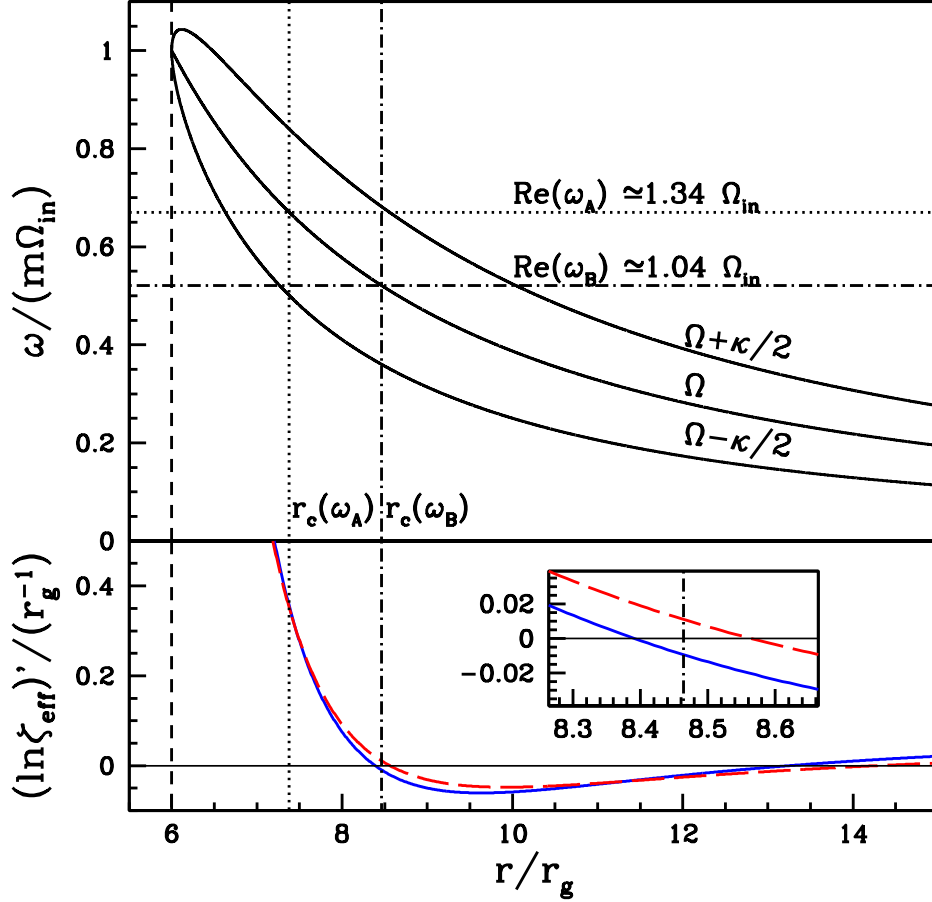
Figure 4. The propagation diagram for disc p-modes with various values of m. The solid curve shows the disc rotation profile Ω, while the various dashed curves show $\Omega + \kappa/m$ (above the Ω curve) and $\Omega - \kappa/m$ (below the Ω curve). The three horizontal lines show the representative values of the mode frequency [in units of $m\Omega_{\rm in}$, where $\Omega_{\rm in} = \Omega(r_{\rm in})$] for $m = 1, 2, 3$ (from bottom to top). The corotation resonance is determined by $\omega/m = \Omega$, the inner Lindblad resonance by $\omega/m = \Omega - \kappa/m$ and the outer Lindblad resonance by $\omega/m = \Omega + \kappa/m$. A mode is trapped between $r_{\rm in} = r_{\rm ISCO}$ and $r_{\rm IL}$, and is evanescent between $r_{\rm IL}$ and $r_{\rm OL}$ (the horizontal dotted lines).

accretion rate increases by a factor of 3. Observationally, it is known that high-frequency QPOs are observed only when the X-ray binary systems reside in the so-called steep power-law spectral state (also called "very high state"), which may corresponds to a very specific range of accretion rates. It is unclear whether our result is consistent with the observed trend in high-frequency QPOs (e.g., Remillard et al. 2002; Remillard & McClintock 2006). Clearly, more sensitive observations (e.g., with future X-ray timing missions; see Barret et al. 2008, Tomsick et al. 2009) would be useful to determine this trend and to search for the possible $m = 4$ mode and the frequency ratios.

Finally, it should be noted that our calculations of global disc modes are still based on rather crude models. The α-discs are phenomenological models, and our results (especially the mode growth rates) depend sensitively on the inner disc boundary conditions (both the l_0 parameter for the background disc and the reflecting boundary condition for the waves). Other potentially important effects (such as turbulence) have not been taken into account. Thus we should treat our specific results (such as those presented in Table 1) only as a demonstration of the basic physical principles, and any comparison with the observations at this point should be taken in this spirit.

Figure 5. The propagation diagram for $m = 2$ disc p-modes and the derivative of the effective disc vortensity profiles. In the lower panel, the ζ_{eff} profiles are shown for disc models with the viscosity prescription $\sigma_{r\phi} = -\alpha P_{\text{gas}}$ (solid curve) and $\sigma_{r\phi} = -\alpha P_{\text{total}}$ (dashed curve), and the other disc parameters are $\dot{M}_{18} = 3$, $l_o/l(r_{\text{in}}) = 0.95$. In the upper panel, the two horizontal lines give the real eigenfrequencies of the 0-node mode, $\text{Re}(\omega) \simeq 1.34\Omega_{\text{in}}$ (for both disc models) and the 1-node mode, $\text{Re}(\omega) \simeq 1.04\Omega_{\text{in}}$ (for the $\sigma_{r\phi} = -\alpha P_{\text{total}}$ disc model only). Note that growing modes can be found only if $d\ln\zeta_{\text{eff}}/dr > 0$ at the corotation, thus the $\text{Re}(\omega) \simeq 1.44\Omega_{\text{in}}$ mode exists for both disc models, while the $\text{Re}(\omega) \simeq 1.04\Omega_{\text{in}}$ mode exists only in one of the disc models. The inset of the lower panel shows a magnified view of the derivative of the effective vortensities at the corotation point of the $\text{Re}(\omega) \simeq 1.04\Omega_{in}$ mode.

REFERENCES

Abramowicz, M.A., Kluzniak, W. 2001, A&A, 374, L19

Abramowitz, M., Stegun, I.A. 1964, Handbook of Mathematical Functions (Dover: New York)

Arras, P., Blaes, O.M. & Turner, N. J., 2006, ApJ, 645, L65

Barret, D. et al. 2008, Proc. SPIE, 7011, 10

Baruteau, C., Masset, F. 2008, ApJ, 672, 1054

Ferreira, B.T., Ogilvie, G.I. 2009, MNRAS, 392, 428

Fu, W., Lai, D. 2009, ApJ, 690, 1386

Goldreich, P., Tremaine, S. 1979, ApJ, 233, 857

Heading, J. 1962, J. Lond. Math. Soc., 37, 195

Horak, J., Karas, V. 2006, A&A, 451, 377

Kato, S., 2001, PASJ, 53, 1

Kato, S., 2003, PASJ, 55, 257

Kato, S., 2008, PASJ, 60, 111

Kato, S. & Fukue, J. 1980, PASJ, 32, 377

Lai, D., Tsang, D. 2009, MNRAS, 393, 979

Li, H., Finn, J.M., Lovelace, R.V.E., Colgate, S.A. 2000, ApJ, 533, 1023

Li, L., Goodman, J., Narayan, R. 2003, ApJ, 593, 980

Li, L., Narayan, R. 2004, ApJ, 601, 414

Lightman, A.P. 1974, ApJ, 194, 419

Lovelace, R.V.E., Li, H., Colgate, S.A., Nelson, A.F. 1999, ApJ, 513, 805

Narayan, R., Goldreich, P., Goodman, J. 1987, MNRAS, 228, 1

Nowak, M. A., Wagoner, R. V. 1991, ApJ, 378, 656

Okazaki, A. T., Kato, S., Fukue, J. 1987, PASJ, 39, 457

O'Neill, S.M., Reynolds, C.S., Miller, C.M. 2009, ApJ, 693, 1100

Ortega-Rodríguez, M., Wagoner, R.V. 2000, ApJ, 537, 922

Paczynski, B., Wiita, P.J. 1980, A&A, 88, 23

Press, W.H., Teukolsky, S.A., Vetterling, W.T., Flannery, B.P. 1998, Numerical Recipes (Cambridge Univ. Press)

Rebusco, P 2008, New Astronomy Reviews, 51, 855

Remillard, R. A. & McClintock, J. E., 2006, ARAA, Vol. 44, pp. 49-92

Remillard, R.A., Muno, M.P., McClintock, J.E., Orosz, J.A. 2002, ApJ 580, 1030

Reynolds, C.S., Miller, M.C. 2009, ApJ, 692, 869

Shakura, N.I., Sunyaev, R.A. 1973, A& A, 24, 337

Shakura, N.I., Sunyaev, R.A. 1976, MNRAS, 175, 613

Tagger, M., Pellat, R. 1999, A&A, 349, 1003

Tagger, M., Varniere, P. 2006, ApJ, 652, 1457

Tomsick, J.A., Remillard, R.A., Kaaret, P., Barret, D., Schnittman, J. 2009, arXiv:0902.4238v1

Tsang, D., Lai, D. 2008, MNRAS, 387, 446

Tsang, D., Lai, D. 2009a, MNRAS, 393, 992

Tsang, D., Lai, D. 2009b, MNRAS, 396, 589

Wagoner, R. V.,1999, Phys. Rep., 311, 259